

Article

The Effectiveness of Ni-Based Bimetallic Catalysts Supported by MgO-Modified Alumina in Dry Methane Reforming

Ahmed A. Ibrahim ^{1,*}, Anis H. Fakeeha ¹, Ahmed E. Abasaed ¹, Irfan Wazeer ¹, Abdulaziz Bentalib ¹, Nadavala Siva Kumar ¹, Jihad K. Abu-Dahrieh ^{2,*} and Ahmed S. Al-Fatesh ^{1,*}

¹ Chemical Engineering Department, College of Engineering, King Saud University, Riyadh 11421, Saudi Arabia; anishf@ksu.edu.sa (A.H.F.); abaseed@ksu.edu.sa (A.E.A.); iwazeer@ksu.edu.sa (I.W.); abentalib@ksu.edu.sa (A.B.); snadavala@ksu.edu.sa (N.S.K.)

² School of Chemistry and Chemical Engineering, Queen's University Belfast, Belfast BT9 5AG, Northern Ireland, UK

* Correspondence: aidid@ksu.edu.sa (A.A.I.); j.abudahrieh@qub.ac.uk (J.K.A.-D.); aalfatesh@ksu.edu.sa (A.S.A.-F.); Tel.: +966-50415854 (A.S.A.-F.)

Abstract: Syngas is produced through the carbon dioxide reforming of methane. The traditional nickel-based catalysts are substantially destroyed by carbon deposition. The reforming reaction was conducted in a tubular microreactor at 700 °C using bimetallic Ni catalysts supported over 37% Al₂O₃ and 63% MgO mixtures. The impregnation process formed the catalysts, which were subsequently examined by N₂-physisorption, XRD, H₂-TPR, TGA, and Raman spectroscopy. The 2.5Ni+2.5Co/37%Al₂O₃+63%MgO bimetallic catalyst, which displayed 72% and 76% conversions of CH₄ and CO₂ over the course of a seven-hour procedure, was discovered to be the most active in DRM. The bimetallic catalyst with the largest weight loss in TGA, 2.5Ni+2.5Fe-MG63, had a loss of 61.3%, a difference of 26% and 21% in the activity performance of CH₄ and CO₂, respectively, of the tested bimetallic Ni catalysts was recorded. The long-time of 30 h on-stream CH₄ and CO₂ conversion reactions for 2.5Ni+2.5Co-MG63 and 2.5Ni+2.5Ce-MG63 catalysts showed the catalysts' high stability. The TPO analysis for the 2.5Ni+2.5Cs-MG63 catalyst showed a peak at 650 °C, attributed to the oxidation of the filamentous carbon, whereas the TPO analysis for the 2.5Ni+2.5Co-MG63 catalyst depicted a peak at 540 °C, ascribed to the presence of amorphous/graphite carbon.

Keywords: bimetallic catalysts; Co; Fe; Ce; Sr; dry reforming of methane



Citation: Ibrahim, A.A.; Fakeeha, A.H.; Abasaed, A.E.; Wazeer, I.; Bentalib, A.; Siva Kumar, N.; Abu-Dahrieh, J.K.; Al-Fatesh, A.S. The Effectiveness of Ni-Based Bimetallic Catalysts Supported by MgO-Modified Alumina in Dry Methane Reforming. *Catalysts* **2023**, *13*, 1420. <https://doi.org/10.3390/catal13111420>

Academic Editors: Leonarda Liotta and Gilles Berhaut

Received: 9 September 2023

Revised: 26 October 2023

Accepted: 31 October 2023

Published: 7 November 2023



Copyright: © 2023 by the authors. Licensee MDPI, Basel, Switzerland. This article is an open access article distributed under the terms and conditions of the Creative Commons Attribution (CC BY) license (<https://creativecommons.org/licenses/by/4.0/>).

1. Introduction

Massive interest in the dry reforming of methane (DRM) has been sparked by the depletion of fossil fuels and the chemical recycling of CH₄ and CO₂ into fuels or chemicals [1–3]. This is because DRM has many benefits, including directly utilizing natural-gas resources [4] and converting greenhouse gases CH₄ and CO₂ into synthesis gas [4–7]. The greenhouse gases are responsible for global warming a major factor in climate change [8]. The DRM reaction Equation (1) generates an H₂/CO ratio of unity, while the reforming of methane Equation (2) produces an H₂/CO ratio of 3. The partial oxidation of methane Equation (3) generates an H₂/CO ratio of 2.



For the Fischer–Tropsch process, which produces long-chain hydrocarbons and oxygenated molecules, a unity H₂/CO ratio is optimal [9,10]. The DRM has advantages over

other reforming reactions, but it also has several disadvantages, which limit its use on a broad scale. Due to CO₂'s thermodynamic stability, it requires considerable energy to oxidize it and create a thermodynamic driving force that produces high yields of H₂ and CO [11]. The H₂/CO ratio falls below unity as a result of the reverse water–gas shift reaction in Equation (4), which also consumes the hydrogen created [12]. In addition, there are side reactions that cause the catalysts to lose their effectiveness. For instance, the Boudouard reaction Equation (5) reduces the CO to carbon, while the CH₄ cracking reaction Equation (6) creates carbon [13,14]. Carbon is produced in both processes, which is detrimental to the efficiency of the dry-reforming catalysts. Both reactions result in the creation of carbon, which is harmful to the effectiveness of the dry-reforming catalysts.



The Ni-based catalysts are found to be promising because they are affordable and readily available [15,16]; however, sintering and coke deposition caused by side reactions, such as CO disproportionation and CH₄ cracking, are drawbacks for Ni catalysts [17]. The catalyst structure can be changed to prevent the creation of carbon. Utilizing supports with strong mechanical properties like alumina, which remain stable at higher temperatures, can endure sintering and suppression [18]. A mixture of Al₂O₃ and MgO supported by Ni, according to a study, inhibits the deposition of carbon [19]. It was also well known that utilizing MgO with basic properties as a support modifier would decrease carbon deposition and increase catalytic stability. The combination of an element with Ni forms bimetallic features, and it was observed that this often acts positively and has therefore attracted wide attention in many eco-friendly and energy-status catalytic applications [20].

Bimetallic catalysts have thus far attracted significant attention, due to the influence of the electronic synergy effect. Because of the increased CO₂ dissociation and metal reducibility, a Ni-Zn/ZrO₂ catalyst is much more active and stable at different temperatures in the dry reforming of the methane reaction [21]. The carbon deposition in the DRM reaction is improved by the common bimetallic catalysts, such as Ni-Co [17,18], Ni-Fe [19–22], Ni-Cu [23], Ni-In [24], Ni-Mo [25], and Ni-Sn [26]. The main strategy to suppress carbon deposition is to increase the concentration of lattice O* on the catalyst surface, which removes filamentous and amorphous carbon. In order to avoid further graphitic carbon production, it is necessary to increase the loading of doped metals, thereby increasing the energy barrier of C–H bond breaking and slowing down the reaction rate. However, a decrease in reaction rate makes the work less efficient, even to stagnate. Various studies indicate that Co can show a nickel-like activity, forming a Ni-Co bimetallic catalyst that exhibits great stability and reduction and effectively suppresses the carbon formation compared to the Ni and Co monometallic catalysts [27,28]. By adjusting the Ni-Co molar ratio, the catalyst has been shown to have reduced carbon accumulation deactivation and enhanced catalytic activity, particularly when the ratio is around 3:1. For instance, the addition of Mo with Ni improves catalytic conversion yields of DRM [22]. Therefore, it could be a good strategy to design bimetallic systems by adding two active metal phases to eliminate significantly the coking and sintering drawbacks that were encountered when a single-element DRM catalyst is employed [20,23]. The synergistic properties of bimetallic systems play a critical part in the catalytic performance and attainment of energy storage of these hybrid materials [23]. Numerous types of research on the DRM reaction have stated that Ni forms an alloy with highly active and carbon-resistant metals, among which Co is an effective option. Indeed, doping Co in the Ni-Co bimetallic catalyst displays high catalytic performance while reducing carbon formation, owing to its high oxygen affinity [24]. Alloying Ni with a second metal was naturally assumed to stabilize metal nanoparticles. Bimetallic Ni-Fe systems have been broadly investigated for DRM [26]. Theofanidis et al. investigated the DRM

stability and impact of Fe in alloying with Ni, and confirmed that a high selectivity toward CO and a CO/H₂ ratio close to unity can be achieved [27].

Commonly, cerium oxide advances catalyst stability, enhances metal dispersion, and upgrades CO₂ activation. Cerium element is a superb promoter for catalytic applications, because of the interconversion capacity of Ce³⁺/Ce⁴⁺, which permits an enhanced oxygen mobility [28]. Some researchers have noted that perovskite oxides containing Sr are resistant to coke deposition in dry reforming; the Sr-doped catalysts exhibit upgraded catalytic performance owing to high oxygen vacancy and activation of the C–H bond [29]. For the purpose of evaluating the activities of the catalysts supported over 63%MgO+Al₂O₃ in the DRM reaction, this paper will study catalysts' chemical, physical, and structural features. For the bimetallic catalysts, a weight loading of 2.5 wt.% was selected for each element. The potential for coking resistance in DRM, the function of bimetallic in optimizing catalytic efficiency, and the production of the synthesis gas are investigated. Various characterization techniques, including N₂ adsorption–desorption, TPR, XRD, Raman, and TGA, were employed to analyze the catalysts.

2. Results

2.1. Surface Description

Table 1 provides a summary of the findings from the BET analysis of the bimetallic samples. The bimetallic samples exhibited similar surface areas and pore volumes, except for the 2.5Ni+2.5Sr-MG63 sample. There is not much variation in the pore size. Figure 1A displays the N₂ adsorption–desorption isotherms. The N₂ physisorption plots in Figure 1A were classified as type IV isotherms by the IUPAC, indicating mesoporous materials with pores that range between 2 and 50 nm diameters, and they have an H3-type adsorption hysteresis loop as a result of slit-shaped pores, which allowed the multilayer of adsorbed N₂ molecules to grow and pack more tightly together [30]. Figure 1B shows mono-modal pore width distribution by BJH Adsorption dV/dlog (D) pore volume method. It confirmed the mesoporosity of the catalysts. The peak maxima lay between 3.7 and 4.0 nm. Table 1 shows the surface area, pore volume, and pore diameters of the bimetallic sample. The 2.5Ni+2.5Sr-MG63 sample assumed the lowest surface area and the lowest pore volume, while the remaining samples displayed similar values.

Table 1. The textural characteristics of the catalysts.

Sample	BET (m ² /g)	P.V. (cm ³ /g)	Pore Size (Å)
2.5Ni+2.5Co-MG63	199	0.309	58.7
2.5Ni+2.5Ce-MG63	201	0.312	56.7
2.5Ni+2.5Fe-MG63	200	0.329	59.8
2.5Ni+2.5Sr-MG63	174	0.283	58.2

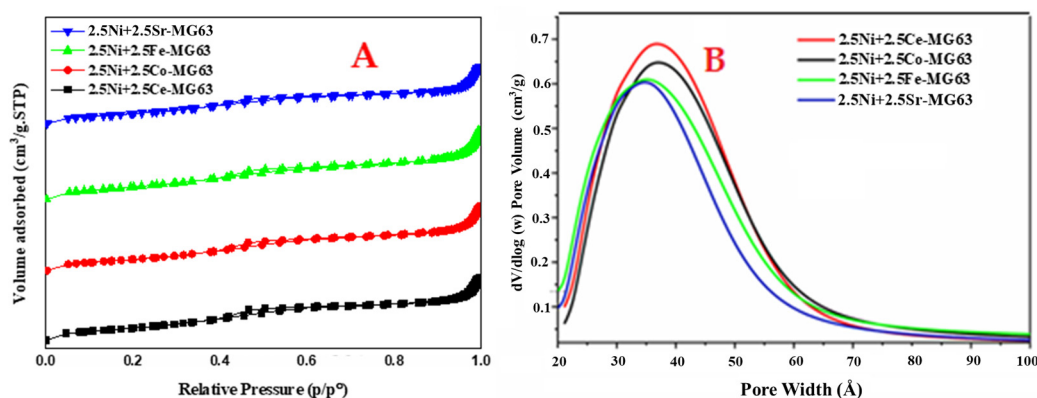


Figure 1. N₂ physical adsorption–desorption isotherm (A) and the pore width distribution via BJH (B).

2.2. TPR

Temperature programmed reduction (H_2 -TPR) was used to test the reducibility of metals to disclose the interaction between the metals and the impact of the reduction process on the structure and composition of the catalysts. Figure 2 displays the H_2 -TPR of the bimetallic catalysts. All the catalysts show two prominent peaks. These reduction peaks at different temperatures indicate the extent of the interaction of the active metals with the support. All the catalysts show peaks at about 945 °C, which can be associated with the metallic exsolution from the stable phases such as $NiAl_2O_4$. The 2.5Ni+2.5Fe-MG63 catalyst has a broad peak at 535 °C, which can be ascribed to the strong interaction of oxides of Ni and Fe with the support. Similarly, in the same region at 686 °C, the 2.5Ni+2.5Ce-MG63 and 2.5Ni+2.5Sr-MG63 show small peaks. On the other hand, the 2.5Ni+2.5Co-MG63 displays a peak at 342 °C, which is characterized by free oxides of Ni and Co on the surface of the support. Because of this type of interaction, the catalyst depicted the best activity. A negative TPR peak at around 200 °C was noticed, and it was determined that it was the result of the metal hydride, which had been created at ambient temperature as a result of the atomic hydrogen being absorbed inside the structure of massive metallic particles. Table 2 shows the quantity of H_2 consumption during the TPR analysis. The 2.5Ni+2.5Co-MG63 sample assumed the highest hydrogen consumption after the 2.5Ni+2.5Fe-MG63 sample. This made the 2.5Ni+2.5Co-MG63 sample the optimum. Because of the presence of several oxidation states of iron, the 2.5Ni+2.5Fe-MG63 sample consumed the highest amount of H_2 to accomplish the stepwise reduction of Fe_2O_3 to Fe through Fe_3O_4 and FeO.

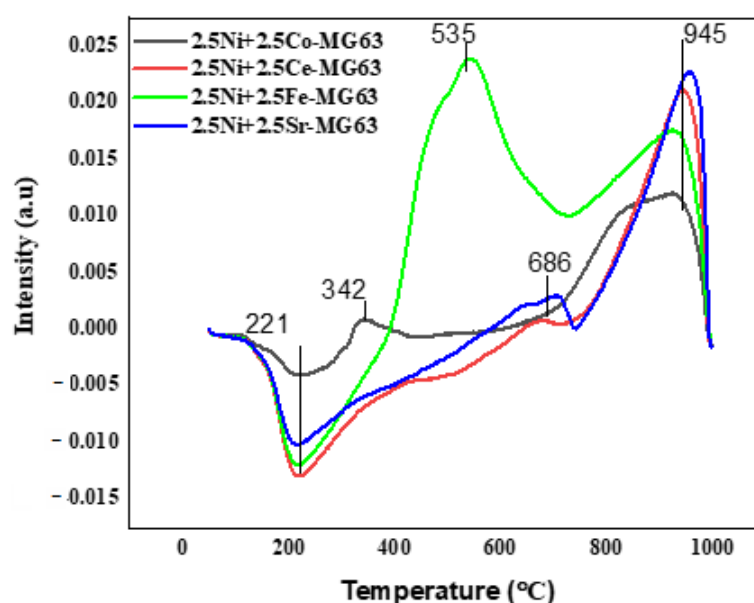


Figure 2. H_2 -Temperature Programmed Reduction spectra of bimetallic catalysts.

Table 2. The amount of H_2 used for the TPR analysis.

Sample	Maximum Temperature (°C)	Quantity (cm ³ /g.STP)	Total Quantity (cm ³ /g.STP)
2.5Ni+2.5Co-MG63	343.4	0.36	19.55
	923.6	19.18	
2.5Ni+2.5Ce-MG63	684.2	0.34	12.47
	944.7	12.13	
2.5Ni+2.5Fe-MG63	543.2	17.46	31.68
	924.3	14.22	
	636.4	0.10	
2.5Ni+2.5Sr-MG63	705.8	1.24	14.57
	957.9	13.12	

2.3. XRD

To examine the crystalline phases in the bimetallic samples, powder X-ray diffraction was employed. Figure 3 shows the diffraction angles for 2.5Ni+2.5Co-MG63, 2.5Ni+2.5Ce-MG63, 2.5Ni+2.5Fe-MG63, and 2.5Ni+2.5Sr-MG63. The 2.5Ni+2.5Co-MG63 catalyst had diffraction peaks at $2\theta = 36.5^\circ$, 43.3° , and 63.0° . The peak at $2\theta = 36.5^\circ$ corresponded to the (111) plane of CoO (JCPDS card, No. 01-075-0419), while the 2.5Ni+2.5Ce-MG63 catalyst had diffraction peaks at $2\theta = 28.6^\circ$, 33.0° , 47.4° , 56.1° , and 63.0° . The diffraction peaks at $2\theta = 28.6^\circ$, 33.0° , 47.4° , and 56.1° were ascribed to CeO₂ (JCPDS 34-0394), while the 2.5Ni+2.5Fe-MG63 and 2.5Ni+2.5Sr-MG63 catalysts had peaks at $2\theta = 35.5^\circ$, 43.3° , and 63.0° . The peak at $2\theta = 35.5^\circ$ corresponds to pure magnetite (Fe₃O₄) (JCPDS card NO. 01-075-0449). In all the catalysts, two diffraction peaks appearing at $2\theta = 43.3^\circ$ and 63.0° could be attributed, respectively, to (113), and (214) crystallographic planes of the cubic γ -alumina phase (JCPDS No. 42-1468).

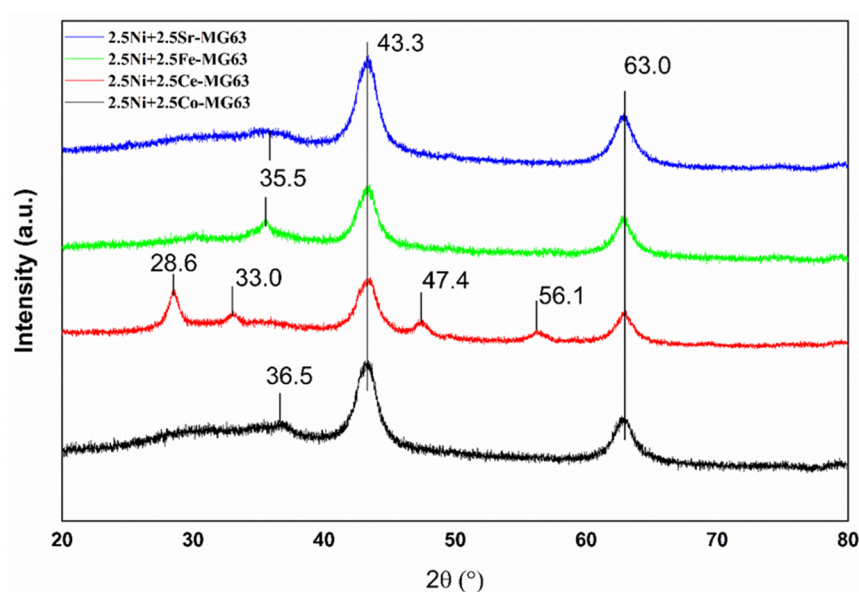


Figure 3. X-ray diffraction.

2.4. TPD

The CO₂-TPD profile presented in Figure 4 may be used to understand the catalyst's fundamental profile as well as its capacity for CO₂ adsorption. Three zones are identified in the CO₂-TPD profile of a catalyst: the low-temperature region (100–150 °C) for weak Brønsted basic sites such as the surface OH[−] group and the intermediate temperature region (200–450 °C) for the medium-strength Lewis base sites, respectively [31]. The CO₂-TPD of the bimetallic catalysts displayed broad and intense peaks in the low to intermediate temperature region. This indicated that the bimetallic catalysts possessed a number of weak- and moderate-strength basic sites. The Sr and Fe bimetallic Ni catalysts have a higher number of basic sites compared to the Co and Ce bimetallic Ni catalysts. The lesser activity performance observed with the Fe and Sr bimetallic Ni catalysts was due to their excessive basicity, which increased the coke deposition. The amount of CO₂ desorbed during the TPD analysis is shown in Table 3. The results show that the Sr and Fe bimetallic Ni catalysts, which exhibit lower activity than the Co and Ce bimetallic Ni catalysts, were more abundant.

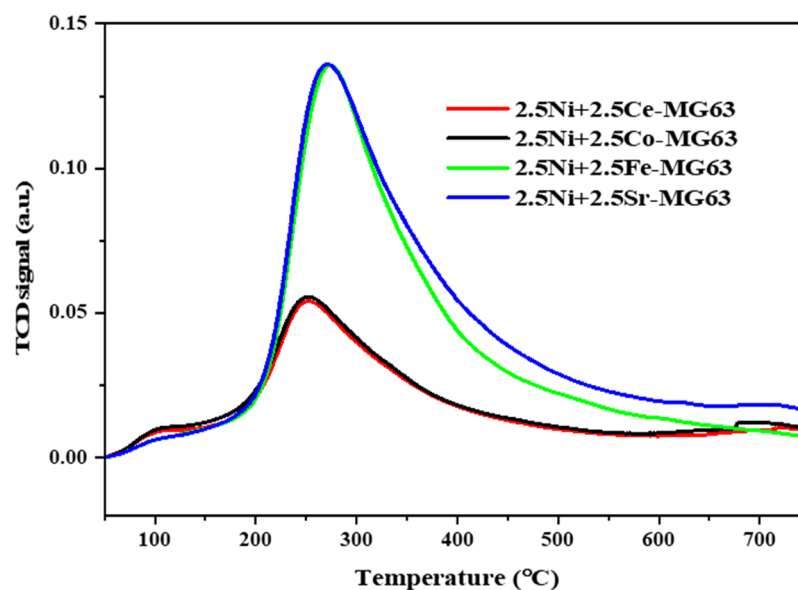


Figure 4. CO₂-Temperature Programmed Desorption profile of Bimetallic catalysts.

Table 3. The quantity of CO₂ desorbed in the TPD.

Sample	Temperature (°C)	Quantity (cm ³ /g.STP)	Total Quantity (cm ³ /g.STP)
2.5Ni+2.5Co-MG63	251.2	10.04	10.43
	696.5	0.39	
2.5Ni+2.5Ce-MG63	252.8	9.66	10.02
	729.1	0.36	
2.5Ni+2.5Fe-MG63	273.6	28.38	28.38
2.5Ni+2.5Sr-MG63	271.0	28.32	28.82
	831.6	0.50	

Raman spectroscopy was used to characterize the structure of the samples. All the Raman spectra displayed the absence of peaks related to carbon, which appears beyond 1000 cm⁻¹. The Raman shift analysis of the fresh samples of bimetallic catalysts was displayed in Figure 5. The peaks that appeared around the Raman shift value of 500 cm⁻¹ were attributable to NiO [32], while the peaks at around 650–700 and 1000 cm⁻¹ were ascribed to Co, Fe and Sr respectively. The peak at 283 cm⁻¹ for the 2.5Ni+2.5Fe-MG63 catalyst was attributable to the Fe₃O₄ [33], while for the 2.5Ni+2.5Co-MG63 catalyst the peak at 282 cm⁻¹ was ascribed to the F_{2g} vibrational modes of the crystalline phase of CO₃O₄ [34]. The high-intensity peak of 2.5Ni+2Ce-MG63 sample was due to the overlapping effect of Ce and NiO. Ni sites are diluted by MgO or another metal oxide, and the Raman peaks are shifted toward a lower frequency [35,36]. So, the shift of the Raman band of NiO was due to the contribution of nearby metal oxides. For Ni-Ce, the appearance of the peak in the range 550–560 cm⁻¹ is easily observable. However, the Raman band is shifted to 476 cm⁻¹ upon incorporation of Fe, suggesting that Fe was inserted into the lattice of NiO. On the other hand, for the Ni-Co, the added Co could form a solid solution as Ni(Co)O. In this case, a broad band around 580 cm⁻¹ assigned to the Co²⁺–O stretching mode appeared, but this signal was overlapped by those of NiO; similarly, the interaction between the NiO and that of the SrO resulted in the appearance of a peak at 559 cm⁻¹.

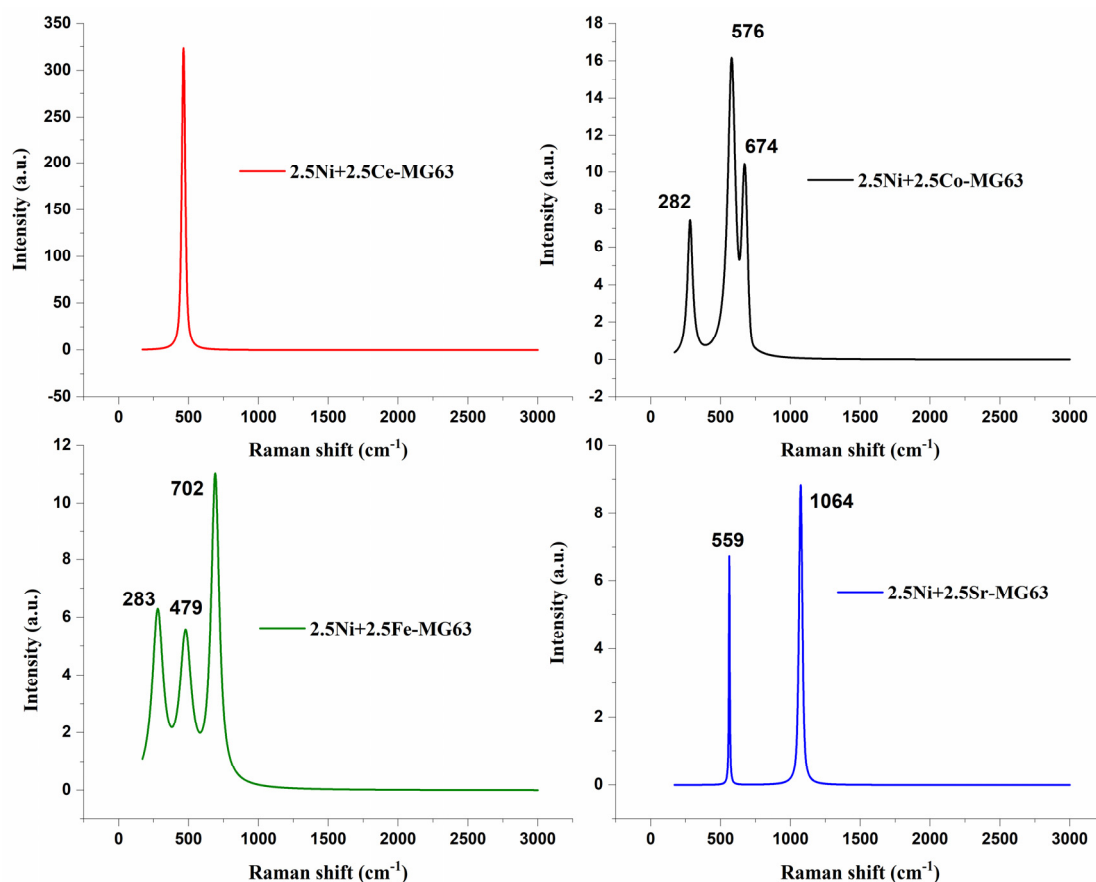


Figure 5. Raman spectroscopy of fresh bimetallic catalysts.

2.5. SEM

SEM analysis was used to evaluate the morphological aspects of the samples. The SEM images of the 2.5Ni+2.5Ce-MG63, 2.5Ni+2.5Co-MG63, and 2.5Ni+2.5Sr-MG63 catalysts are presented in Figure 6. From the figures, quite homogeneous distributions of oxide particles were observed in fresh catalysts, while for the used catalysts, aggregation of clusters due to coke and sintering after the reaction (7 h) was displayed.

2.6. TEM

Figure 7 shows the fresh and the spent TEM images of the 2.5Ni+2.5Co-MG63 catalyst. The image of the fresh catalyst displays the good distribution of the active metal particles, while the used TEM shows the formation of slight graphitic carbon, as depicted by the TPO characterization analysis.

2.7. Catalytic Activity

Before evaluating commercially produced catalysts, a blank experiment to test catalytic performance was conducted using an empty stainless-steel reactor without catalysts under the same feed ratio and reaction temperature of 700 °C. The CH₄ and CO₂ conversions of 1.5% and 0.3%, respectively, were obtained; therefore, the metallic reactor had an insignificant effect. The CH₄ and CO₂ conversions are illustrated in Figure 8. The 2.5Ni+2.5Co-MG63 sample gave a conversion of CH₄ about 74% higher than the other bimetallic samples. The 2.5Ni+2.5Co-MG63 sample also gave the highest CO₂ conversion, of about 78%, whereas the 2.5Ni+2.5Ce-MG63 displayed higher CO₂ conversion values, of about 74%, than 2.5Ni+2.5Fe-MG63 and 2.5Ni+2.5Sr-MG63. The lowest activity performance was recorded by the 2.5Ni+2.5Sr-MG63. In all the catalyst samples, the conversion values of CO₂ are higher than the corresponding CH₄ value. The side reaction of the reverse water–gas shift may have contributed to this outcome by reacting with the produced H₂,

as depicted in Equation (4) [37]. The active site of DRM is metallic Ni. 2.5Ni2.5Fe/Mg63 catalyst has the highest consumption of H₂ and the highest interaction of CO₂ but the DRM activity of 2.5Ni2.5Fe/Mg63 is less than the 2.5Ni2.5Co/Mg63. This indicates that, despite good interaction with CO₂, the catalytic active sites are not much exposed for excelling the DRM due to the shading of Ni by Fe. 2.5Ni2.5Co/Mg63 has relatively less H₂-consumption and CO₂ consumption (less reducibility and less extent of interaction with CO₂) than 2.5Ni2.5Fe/Mg63 but the DRM activity of the catalyst is highest. This indicates that, with a combination of Co, the catalytic active sites Ni are well exposed, and it excels in the DRM reaction even though it has lower number of active sites than 2.5Ni2.5Fe/Mg63. The reducible species over 2.5Ni2.5Ce/Mg63 and 2.5Ni2.5Sr/Mg63 catalysts are much lower than 2.5Ni2.5Fe/Mg63 and 2.5Ni2.5Co/Mg63 catalysts. So, the catalytic activities of these catalysts toward DRM are inferior.

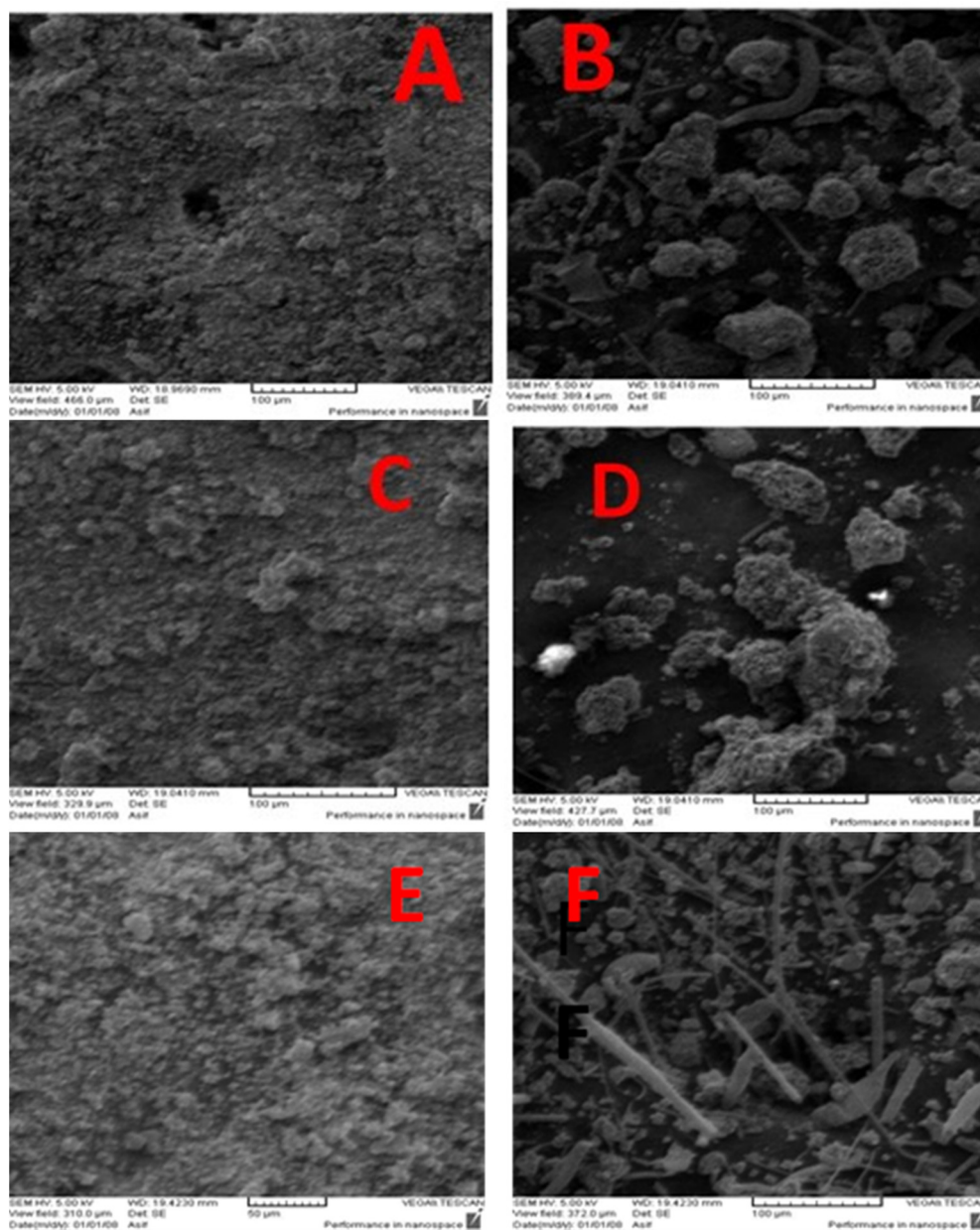


Figure 6. SEM images of 2.5Ni+2.5Ce-MG63 (A,B), 2.5Ni+2.5Co-MG63 (C,D), 2.5Ni+2.5Sr-MG63 (E,F), where A, C, E (fresh) and B, D, F (used) catalysts.

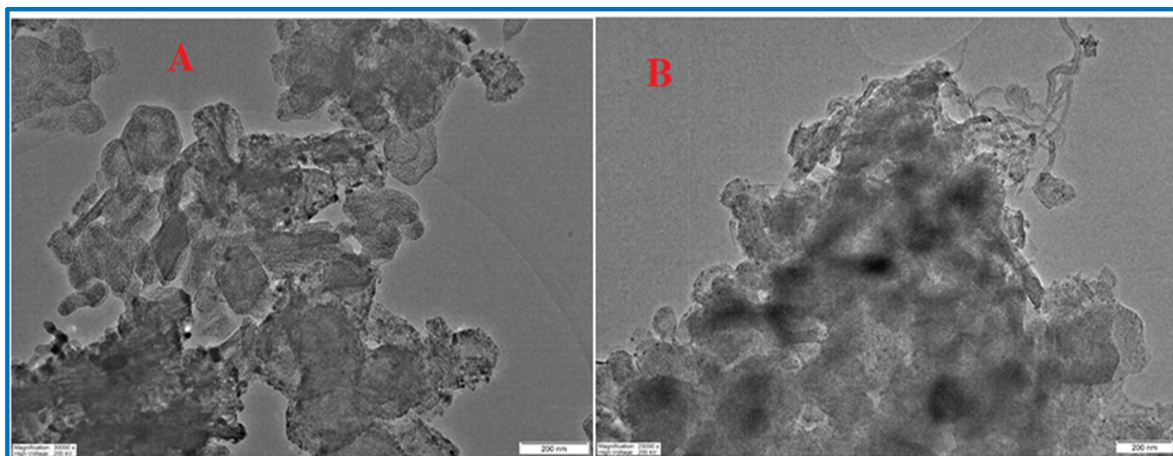


Figure 7. TEM image of 2.5Ni+2.5Co-MG63 (A) Fresh, (B) Used.

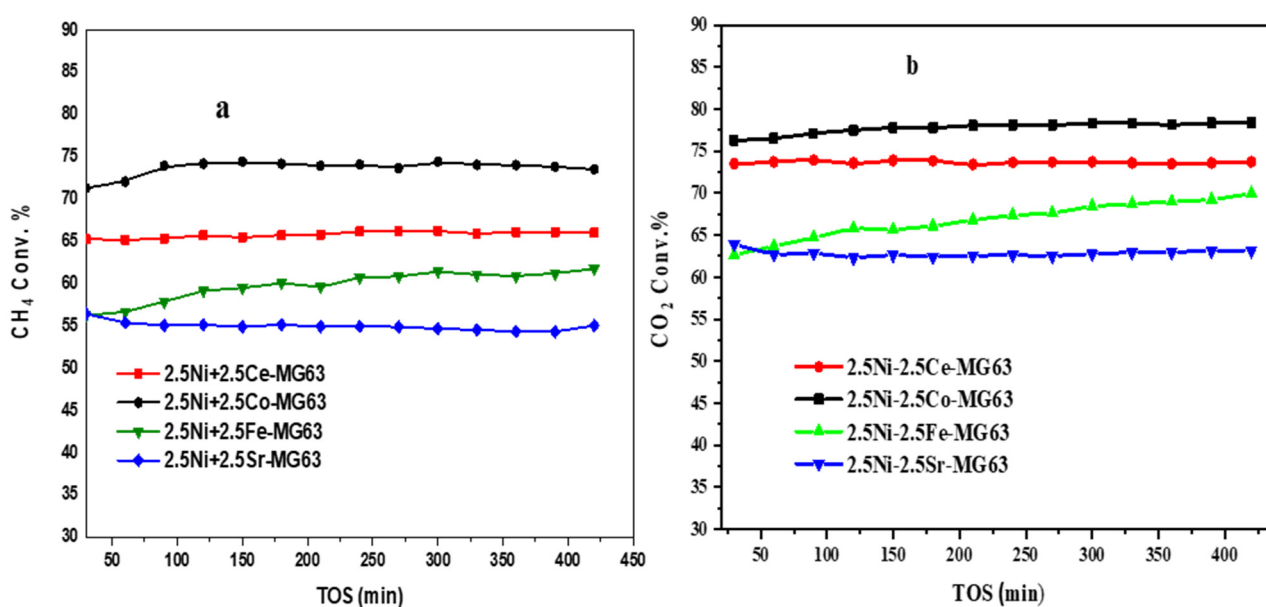


Figure 8. Conversions of (a) CH₄ and (b) CO₂ as a result of TOS (reaction circumstances: CH₄/CO₂/N₂ = 3/3/1 (v/v/v); GHSV = 42,000 mL/g_{cat}/h; M_{cat} = 0.1g; t = 700 °C).

2.8. TGA

The amount of carbon that had been deposited was calculated using the thermogravimetric analysis. Figure 9 displays the weight loss of the carbon deposits on the catalyst samples as a fraction of the total weight loss. The catalyst sample 2.5Ni+2.5Fe-MG63 indicated a maximum weight loss of 61.3% at a reaction temperature of 700 F and a reaction duration of 7 h, followed by 2.5Ni+2.5Co-MG63, 2.5Ni+2.5Sr-MG63, and 2.5Ni+2.5Ce-MG63 catalysts, which produced 58%, 27.2%, and 23.7% weight loss, respectively. The 2.5Ni+2.5Co-MG63 catalyst had a significant weight loss of carbon deposited on it, which was in perfect agreement with the catalyst's high activity.

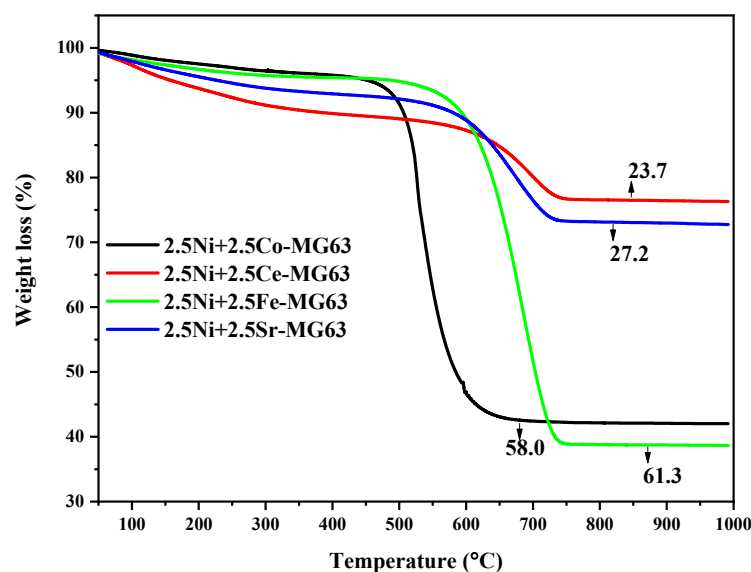


Figure 9. TGA curve for temperature gravimetric analysis of the used catalyst after 7 h time on-stream.

For verification of stability and suitability for industrial operation, the long-time on-streams of CH_4 and CO_2 conversion reactions for 2.5Ni+2.5Co-MG63 and 2.5Ni+2.5Ce-MG63 catalysts were performed for 30 h, as shown in Figure 10. The result displays the catalysts maintained their activities with negligible deactivation and hence established the good stability of the catalysts. The TPO analysis for the same catalysts after the 30 h reaction at 700 °C temperature was carried out and depicted in Figure 11. The TPO was done to ascertain the overall quantity and reactivity of the carbon deposit on the surface of catalysts. The 2.5Ni+2.5Co-MG63 catalyst's TPO curve showed the existence of a peak with a maximum temperature of 540 °C, assigned to the presence of amorphous/graphite carbon [38], while the 2.5Ni+2.5Cs-MG63 catalyst showed the presence of a peak with a maximum temperature of 650 °C, attributed to the oxidation of the filamentous carbon. Table 4 compares the effectiveness of the present work to those in the past. The result show that a good catalyst is developed.

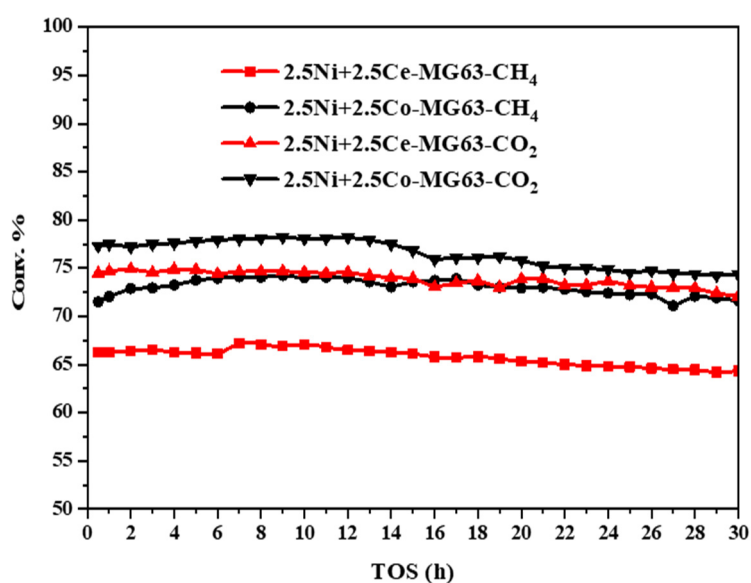


Figure 10. Conversions of CH_4 and CO_2 as a result of long-time on-stream (reaction circumstances: $\text{CH}_4/\text{CO}_2/\text{N}_2 = 3/3/1$ (v/v/v); GHSV = 42,000 mL/g_{cat}/h; M_{cat} = 0.1 g; t = 700 °C).

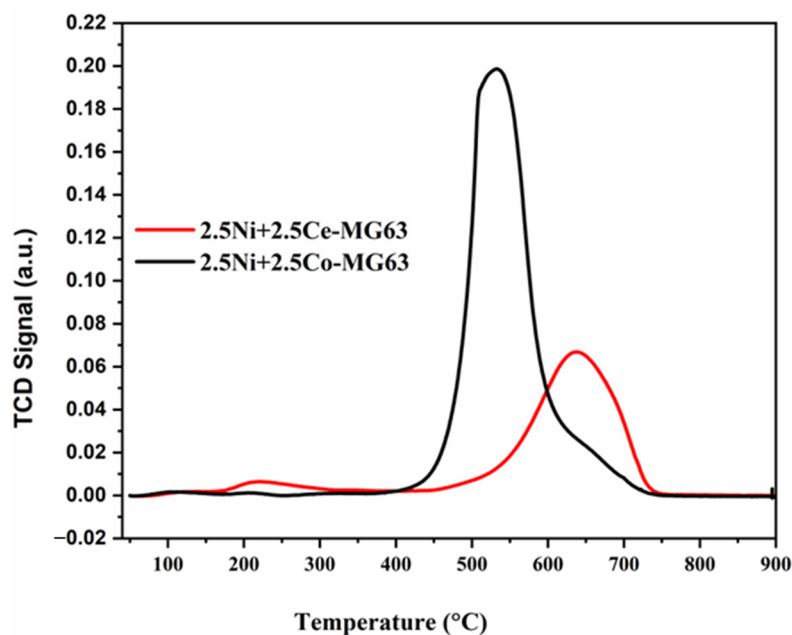


Figure 11. TPO profile of 2Ni+2.5Ce-MG63 and 2Ni+2.5Ce-MG63 catalysts after 30 h of reaction.

Table 4. Performance assessment of the current study in comparison to past studies.

Cat-Name (°C)	CH ₄ /CO ₂	GHSV (mL/hg _{cat})	RT (°C)	CH ₄ -Conv. (%)	CO ₂ -Conv. (%)	REF.
Ni-Mn/CeO ₂ -ZrO ₂	1:1	20,000	600	39	40	[34]
Na-Ni/ZrO ₂	68:31	12,000	675	25	55	[37]
Ni-Cu/Mg(Al)O	1:1	60,000	600	50	57	[38]
Ni-Co/SiO ₂	1:1	700	24,000	30	40	[39]
Ni-Pt/Ti-SBA-15	1:1	700	36,000	57	60	[40]
Ni-Cd	1:1	700	12,000	50	60	[41]
Ni-Mo/Al ₂ O ₃	1:1	20,000	900	60	70	[42]
2.5Ni+2.5Co-MG63	25:25	36,000	700	72	76	This work

3. Materials

All the chemicals were purchased from commercial sources and used without further treatment. Nickel nitrate hexahydrate Ni(NO₃)₂·6H₂O, cobalt nitrate hexahydrate Co(NO₃)₂·6H₂O, iron nitrate nonahydrate Fe(NO₃)₃·9H₂O, cerium nitrate hexahydrate Ce(NO₃)₃·6H₂O, and strontium nitrate hexahydrate Sr(NO₃)₂·6H₂O were purchased from Alfa Aesar (Heysham, Britain). 63%MgO+37%Al₂O₃ support was obtained as a gift from SASOL Anckelmannsplatz 1 (Hamburg, Germany). deionized water, crucible, and crusher.

3.1. Preparation of Catalysts

2.5 wt.% of Ni and 2.5 wt.% Co, 2.5 wt.% Ce, 2.5 wt.% Fe, and 2.5 wt.% Sr were synthesized to form bimetallic Ni by a simple wet impregnation method. 0.95 g of support was dispersed in 100 mL of deionized water at room temperature for 20 min. Then, appropriate amounts of nickel nitrate hexahydrate, cobalt nitrate hexahydrate, iron nonahydrate, cerium nitrate hexahydrate, or strontium nitrate hexahydrate were added to form bimetallic compounds of Ni, and the output product was stirred at 80 °C until dry. The obtained solid sample was first calcined in air at 600 °C for 3 h.

3.2. Catalytic Evaluation

In a continuous-flow fixed-bed reactor (30 cm long and 0.94 cm in diameter) operating at 1 atm, the catalyst's activity (0.1 g) was measured. A thermocouple was fastened to the catalyst's central bed in order to gauge the reaction's temperature. Before the response

began, H₂ was added to the catalysts at a flow rate of 30 mL/min for an hour at 700 °C. The reactor was then purged with flowing N₂ at a rate of 20 mL/min for 20 min at 700 °C to eliminate any leftover H₂. Before the N₂ purge was halted, the reactor temperature was allowed to rise to 800 °C. CH₄/CO₂/N₂ was the input gas. Throughout the process, the flow was maintained at 70 mL/min. with a space velocity of 42,000 mL/hg_{cat}. A 30/30/10 volume ratio was used. To evaluate the concentration of the reactor's products and unconverted feed gases, a thermal conductivity detector and an online GC (GC-Shimadzu 2014, Kyoto, Japan) outfitted with two columns (Porapak Q and Molecular Sieve 5A) were coupled to the reactor. The effectiveness of the activity was assessed using Equations (7) and (8).

$$\text{Methane conversion(\%)} = \frac{\text{CH}_{4,\text{in}} - \text{CH}_{4,\text{out}}}{\text{CH}_{4,\text{in}}} \times 100 \quad (7)$$

$$\text{Carbon dioxide conversion(\%)} = \frac{\text{CO}_{2,\text{in}} - \text{CO}_{2,\text{out}}}{\text{CO}_{2,\text{in}}} \times 100 \quad (8)$$

3.3. Catalyst Characterization

The specific surface areas of the catalysts were measured using nitrogen physisorption at 196 °C. Using a Micromeritics Tristar II 3020 instrument (Micromeritics, Atlanta, GA, USA), the surface area (BET) was calculated using the Brunauer–Emmett–Teller technique (Micromeritics, Atlanta, GA, USA). The quantity of carbon deposited on spent was evaluated using a Shimadzu thermal gravimetric analysis (TGA) system in air, catalysts Shimadzu Corporation's TGA-51 (Shimadzu Corporation, Kyoto, OP, Japan). Using a laser Raman (NMR-4500-JASCO, Tokyo, Japan) spectrometer, the level of graphitization and the kind of carbon over the catalysts were assessed. The excitation laser utilized had a wavelength of 532 nm. The structure of the employed materials was documented using a TEM (transmission electron microscope) (120 kV JEOL JEM-2100F-Akishima, Tokyo, Japan). TEM micrographs were captured at 120 kV. To investigate the crystal phases and the structure of the fresh catalysts, an X-ray diffractometer was employed. A Miniflex Rigaku diffractometer (Rigaku, Bahrain, Saudi Arabia) was used for the experiment, producing Cu K α X-ray radiation while operating at 40 kV and 40 mA. A 2 h angle span of 10–85 and a step magnitude of 0.01 were used to collect the data. Micromeritics Auto Chem II 2920 (H₂-TPR) equipment (Micromeritics, Atlanta, GA, USA) was used to do the temperature-programmed reduction. The catalysts were heated for an hour at 200 °C in an argon environment before the tests, and they were then cooled to room temperature. For H₂-TPR, 0.07 g of the sample was heated to 1000 °C and passed through an H₂/Ar (*v/v*, 10/90) gas mixture at a rate of 40 mL/min. The structure of the produced catalysts was investigated via SEM analysis utilizing a Philips XL-30-FEG equipment (Eindhoven, The Netherlands). Utilizing the Micromeritics Auto Chem II 2920 (Atlanta, GA, USA), temperature-programmed oxidation (TPO) analysis was carried out. Prior to cooling to room temperature, the used catalyst was pre-treated with argon at 150 °C for 30 min. The catalyst's temperature was then increased from 50 to 1000 °C while being exposed to a 10% oxidizing gas/He combination (flow rate of 40 mL/min).

4. Conclusions

Syngas was produced through the CO₂ reforming of methane (DRM) using bimetallic Ni catalysts supported on 63% MgO and 37% alumina. Co, Ce, Fe, and Sr are the bimetallic Ni catalysts tested. The catalyst 2.5Ni+2.5Co-MG63 produced the maximum catalytic activity for DRM. Over seven hours, there were 73% and 76%, respectively, CH₄ and CO₂ conversions. The catalyst gave the highest weight loss, of 58%, after the 2.5Ni+2.5Fe-MG63. This could be related to the high activity of the sample. The difference of activity performance of CH₄ and CO₂ of the tested bimetallic Ni catalysts generated values of 26% and 21% respectively. The long-time on stream of CH₄ and CO₂ conversion reactions for

2.5Ni+2.5Co-MG63 and 2.5Ni+2.5Ce-MG63 catalysts displayed that the catalysts upheld their activities with negligible deactivation and hence established the good stability of the catalysts. The TPO analysis of spent 2.5Ni+2.5Co-MG63 and 2.5Ni+2.5Ce-MG63 catalysts after 30 h reaction at 700 °C temperature determined the overall quantity and reactivity of the carbon deposit on the surface of catalysts: amorphous/graphite carbon for the 2.5Ni+2.5Co-MG63 catalyst and filamentous carbon for 2.5 Ni + 2.5 Cs-MG63 catalyst.

Author Contributions: A.S.A.-F. and A.A.I.: writing—original draft, supervision, data curation, methodology, validation, review, A.H.F. and A.B.: project administration, investigation, conceptualization, formal analysis; A.E.A., N.S.K., J.K.A.-D. and I.W.: formal analysis, review, editing. All authors have read and agreed to the published version of the manuscript.

Funding: Deputyship for Research and Innovation, “Ministry of Education” in Saudi Arabia for funding this research (IFKSUOR3-544-1), King Saud University, Riyadh, Saudi Arabia.

Data Availability Statement: Not applicable.

Acknowledgments: The authors extend their appreciation to the Deputyship for Research and Innovation, “Ministry of Education” in Saudi Arabia for funding this research (IFKSUOR3-544-1).

Conflicts of Interest: The authors declare that they have no competing interests.

References

1. Yan, X.; Hu, T.; Liu, P.; Li, S.; Zhao, B.; Zhang, Q.; Jiao, W.; Chen, S.; Wang, P.; Lu, J.; et al. Highly Efficient and Stable Ni/CeO₂-SiO₂ Catalyst for Dry Reforming of Methane: Effect of Interfacial Structure of Ni/CeO₂ on SiO₂. *Appl. Catal. B Environ.* **2019**, *246*, 221–231. [[CrossRef](#)]
2. Cao, P.; Adegbite, S.; Zhao, H.; Lester, E.; Wu, T. Tuning Dry Reforming of Methane for F-T Syntheses: A Thermodynamic Approach. *Appl. Energy* **2018**, *227*, 190–197. [[CrossRef](#)]
3. Usman, M.; Daud, W.M.A.W.; Abbas, H.F. Dry Reforming of Methane: Influence of Process Parameters—A Review. *Renew. Sustain. Energy Rev.* **2015**, *45*, 710–744. [[CrossRef](#)]
4. Amin, R.; Liu, B.; Huang, Z.B.; Zhao, Y.C. Hydrogen and Syn Gas Production via CO₂ Dry Reforming of Methane over Mg/La Promoted Co-Ni/MSU-S Catalyst. *Int. J. Hydrogen Energy* **2016**, *41*, 807–819. [[CrossRef](#)]
5. Al-Fatesh, A.S.; Atia, H.; Ibrahim, A.A.; Fakeeha, A.H.; Singh, S.K.; Labhsetwar, N.K.; Shaikh, H.; Qasim, S.O. CO₂ Reforming of CH₄: Effect of Gd as Promoter for Ni Supported over MCM-41 as Catalyst. *Renew. Energy* **2019**, *140*, 658–667. [[CrossRef](#)]
6. Furkan, H.B.; Rakibul Hasan, K.M.; Uddin, M.J. Greenhouse Gas Emission, GDP, Tertiary Education, and Rule of Law: A Comparative Study between High-Income and Lower-Middle Income Countries. *Heliyon* **2023**, *9*, e16265. [[CrossRef](#)] [[PubMed](#)]
7. Hamza Fakeeha, A.; Sadeq Al-Fatesh, A.; Aidid Ibrahim, A.; Elhag Abasaheed, A. CO₂ Reforming of CH₄ over Ni-Catalyst Supported on Yttria Stabilized Zirconia. *J. Saudi Chem. Soc.* **2021**, *25*, 101244. [[CrossRef](#)]
8. Yentekakis, I.V.; Dong, F. Grand Challenges for Catalytic Remediation in Environmental and Energy Applications Toward a Cleaner and Sustainable Future. *Front. Environ. Chem.* **2020**, *1*, 1–14. [[CrossRef](#)]
9. Zhang, M.; Liu, J.; Zhang, Y.H.; Wang, L.; Li, J.L.; Hong, J.P. Preparation of Highly Dispersed Silicon Spheres Supported Cobalt-Based Catalysts and Their Catalytic Performance for Fischer-Tropsch Synthesis. *J. Fuel Chem. Technol.* **2023**, *51*, 608–615. [[CrossRef](#)]
10. Pratschner, S.; Hammerschmid, M.; Müller, S.; Winter, F. Evaluation of CO₂ Sources for Power-to-Liquid Plants Producing Fischer-Tropsch Products. *J. CO₂ Util.* **2023**, *72*, 102508. [[CrossRef](#)]
11. Aramouni, N.A.K.; Touma, J.G.; Tarboush, B.A.; Zeaiter, J.; Ahmad, M.N. Catalyst Design for Dry Reforming of Methane: Analysis Review. *Renew. Sustain. Energy Rev.* **2018**, *82*, 2570–2585. [[CrossRef](#)]
12. Nikoo, M.K.; Amin, N.A.S. Thermodynamic Analysis of Carbon Dioxide Reforming of Methane in View of Solid Carbon Formation. *Fuel Process. Technol.* **2011**, *92*, 678–691. [[CrossRef](#)]
13. Al-Zahrani, S.A.; Al-Fatesh, A.S.; Kaydouh, M.N.; Al Otaibi, A.; Francesco, F.; Fakeeha, A.H.; El Hassan, N. High Carbon-Resistant Nickel Supported on Yttria-Zirconia Catalysts for Syngas Production by Dry Reforming of Methane: The Promoting Effect of Cesium. *Alexandria Eng. J.* **2023**, *74*, 371–386. [[CrossRef](#)]
14. Abasaheed, A.E.; Al-Fatesh, A.S.; Naem, M.A.; Ibrahim, A.A.; Fakeeha, A.H. Catalytic Performance of CeO₂ and ZrO₂ Supported Co Catalysts for Hydrogen Production via Dry Reforming of Methane. *Int. J. Hydrogen Energy* **2015**, *40*, 6818–6826. [[CrossRef](#)]
15. Muraleedharan Nair, M.; Kaliaguine, S. Structured Catalysts for Dry Reforming of Methane. *New J. Chem.* **2016**, *40*, 4049–4060. [[CrossRef](#)]
16. Abdullah, B.; Abd Ghani, N.A.; Vo, D.V.N. Recent Advances in Dry Reforming of Methane over Ni-Based Catalysts. *J. Clean. Prod.* **2017**, *162*, 170–185. [[CrossRef](#)]
17. Palanichamy, K.; Umasankar, S.; Ganesh, S.; Sasirekha, N. Highly Coke Resistant Ni-Co/KCC-1 Catalysts for Dry Reforming of Methane. *Int. J. Hydrogen Energy* **2023**, *48*, 11727–11745. [[CrossRef](#)]

18. Almeida, C.M.R.; Ghica, M.E.; Durães, L. An Overview on Alumina-Silica-Based Aerogels. *Adv. Colloid Interface Sci.* **2020**, *282*, 102189. [\[CrossRef\]](#)
19. Wang, S.; Lu, G.Q.M. CO₂ Reforming of Methane on Ni Catalysts: Effects of the Support Phase and Preparation Technique. *Appl. Catal. B Environ.* **1998**, *16*, 269–277. [\[CrossRef\]](#)
20. Bian, Z.; Das, S.; Wai, M.H.; Hongmanorom, P.; Kawi, S. A Review on Bimetallic Nickel-Based Catalysts for CO₂ Reforming of Methane. *ChemPhysChem* **2017**, *18*, 3117–3134. [\[CrossRef\]](#)
21. Velisoju, V.K.; Virpurwala, Q.J.S.; Attada, Y.; Bai, X.Q.; Davaasuren, B.; Hassine, M.B.; Yao, X.L.; Lezcano, G.; Kulkarni, S.R.; Castano, P. Overcoming the kinetic and deactivation limitations of Ni catalyst by alloying it with Zn for the dry reforming of methane. *J. CO₂ Util.* **2023**, *75*, 102573. [\[CrossRef\]](#)
22. Gaillard, M.; Virginie, M.; Khodakov, A.Y. New Molybdenum-Based Catalysts for Dry Reforming of Methane in Presence of Sulfur: A Promising Way for Biogas Valorization. *Catal. Today* **2017**, *289*, 143–150. [\[CrossRef\]](#)
23. De, S.; Zhang, J.; Luque, R.; Yan, N. Ni-Based Bimetallic Heterogeneous Catalysts for Energy and Environmental Applications. *Energy Environ. Sci.* **2016**, *9*, 3314–3347. [\[CrossRef\]](#)
24. Hu, Y.H.; Ruckenstein, E. Comment on “Dry Reforming of Methane by Stable Ni-Mo Nanocatalysts on Single-Crystalline MgO”. *Science* **2020**, *368*, 777–781. [\[CrossRef\]](#) [\[PubMed\]](#)
25. Luisetto, I.; Tuti, S.; Di Bartolomeo, E. Co and Ni Supported on CeO₂ as Selective Bimetallic Catalyst for Dry Reforming of Methane. *Int. J. Hydrogen Energy* **2012**, *37*, 15992–15999. [\[CrossRef\]](#)
26. Zhang, T.; Liu, Z.; Zhu, Y.A.; Liu, Z.; Sui, Z.; Zhu, K.; Zhou, X. Dry Reforming of Methane on Ni-Fe-MgO Catalysts: Influence of Fe on Carbon-Resistant Property and Kinetics. *Appl. Catal. B Environ.* **2020**, *264*, 118497. [\[CrossRef\]](#)
27. Theofanidis, S.A.; Galvita, V.V.; Poelman, H.; Marin, G.B. Enhanced Carbon-Resistant Dry Reforming Fe-Ni Catalyst: Role of Fe. *ACS Catal.* **2015**, *5*, 3028–3039. [\[CrossRef\]](#)
28. Papavasiliou, J.; Rawski, M.; Vakros, J.; Avgouropoulos, G. A Novel Post-Synthesis Modification of CuO-CeO₂ Catalysts: Effect on Their Activity for Selective CO Oxidation. *ChemCatChem* **2018**, *10*, 2096–2106. [\[CrossRef\]](#)
29. Yang, E.H.; Noh, Y.S.; Ramesh, S.; Lim, S.S.; Moon, D.J. The Effect of Promoters in La_{0.9}M_{0.1}Ni_{0.5}Fe_{0.5}O₃ (M = Sr, Ca) Perovskite Catalysts on Dry Reforming of Methane. *Fuel Process. Technol.* **2015**, *134*, 404–413. [\[CrossRef\]](#)
30. Thommes, M.; Kaneko, K.; Neimark, A.V.; Olivier, J.P.; Rodriguez-Reinoso, F.; Rouquerol, J.; Sing, K.S.W. Physisorption of Gases, with Special Reference to the Evaluation of Surface Area and Pore Size Distribution (IUPAC Technical Report). *Pure Appl. Chem.* **2015**, *87*, 1051–1069. [\[CrossRef\]](#)
31. Al-Fatesh, A.S.; Kumar, R.; Kasim, S.O.; Aidid, A.; Anis, I.; Fakeeha, H.; Abasaeed, A.E.; Atia, H.; Armbruster, U.; Kreyenschulte, C.; et al. Effect of Cerium Promoters on an MCM-41-Supported Nickel Catalyst in Dry Reforming of Methane. *Cite This Ind. Eng. Chem. Res* **2021**, *2022*, 174. [\[CrossRef\]](#)
32. Mironova-Ulmane, N.; Kuzmin, A.; Sildos, I.; Puust, L.; Grabis, J. Magnon and Phonon Excitations in Nanosized NiO. *Latv. J. Phys. Tech. Sci.* **2019**, *56*, 61–72. [\[CrossRef\]](#)
33. Shebanova, O.N.; Peter Lazor, P. Raman study of magnetite (Fe₃O₄): Laser-induced thermal effects and oxidation. *J. Raman Spectrosc.* **2003**, *34*, 845–852. [\[CrossRef\]](#)
34. Tang, C.-W.; Wang, C.-B.; Chien, S.-H. Characterization of cobalt oxides studied by FT-IR, Raman, TPR and TG-MS. *Thermochim. Acta* **2008**, *473*, 68–73. [\[CrossRef\]](#)
35. Cazzanelli, E.; Kuzmin, A.; Mariotto, G.; Mironova-Ulmane, N. Study of Vibrational and Magnetic Excitations in NiMg1-CO Solid Solutions by Raman Spectroscopy. *J. Phys. Condens. Matter* **2003**, *15*, 2045–2052. [\[CrossRef\]](#)
36. Funkenbusch, E.F.; Cornilsen, B.C. Two-Magnon Raman Scattering in Calcium Doped NiO. *Solid State Commun.* **1981**, *40*, 707–710. [\[CrossRef\]](#)
37. González-Castaño, M.; Dorneanu, B.; Arellano-García, H. The Reverse Water Gas Shift Reaction: A Process Systems Engineering Perspective. *React. Chem. Eng.* **2021**, *6*, 954–976. [\[CrossRef\]](#)
38. Stroud, T.; Smith, T.J.; Le Saché, E.; Santos, J.L.; Centeno, M.A.; Arellano-García, H.; Odriozola, J.A.; Reina, T.R. Chemical CO₂ Recycling via Dry and Bi Reforming of Methane Using Ni-Sn/Al₂O₃ and Ni-Sn/CeO₂-Al₂O₃ Catalysts. *Appl. Catal. B Environ.* **2018**, *224*, 125–135. [\[CrossRef\]](#)
39. Zou, Z.; Zhang, T.; Lv, L.; Tang, W.; Zhang, G.; Gupta, R.K.; Wang, Y.; Tang, S. Preparation adjacent Ni-Co bimetallic nano catalyst for dry reforming of methane. *Fuel* **2023**, *343*, 128013. [\[CrossRef\]](#)
40. Palanichamy, K.; Sasirekha, N. Dry reforming of methane using bimetallic Pt-Ni/TiSBA-15: Effect of Si/Ti ratio on catalytic activity and stability. *Int. J. Hydrogen Energy* **2023**, *48*, 31126–31141. [\[CrossRef\]](#)
41. Mohandessi, M.; Tavakolian, M.; Rahimpour, M.R. Cadmium as a robust and novel promoter over Ni@γ-Al₂O₃ catalysts in dry methane reforming. *ACS Appl. Energy Mater.* **2023**, *6*, 8209–8220. [\[CrossRef\]](#)
42. Yao, L.; Galvez, M.E.; Hu, C.; Da Costa, P. Mo-Promoted Ni/Al₂O₃ Catalyst for Dry Reforming of Methane. *Int. J. Hydrogen Energy* **2017**, *42*, 23500–23507. [\[CrossRef\]](#)

Disclaimer/Publisher’s Note: The statements, opinions and data contained in all publications are solely those of the individual author(s) and contributor(s) and not of MDPI and/or the editor(s). MDPI and/or the editor(s) disclaim responsibility for any injury to people or property resulting from any ideas, methods, instructions or products referred to in the content.